Applied Ocean Research 107 (2021) 102486

Contents lists available at ScienceDirect

Applied Ocean Research

journal homepage: www.elsevier.com/locate/apor

Approach-angle-based three-dimensional indirect adaptive fuzzy path following of under-actuated AUV with input saturation☆

Jialei Zhang [a], Xianbo Xiang [*,a,b,d], Lionel Lapierre [c], Qin Zhang [d], Weijia Li [a]

[a] School of Naval Architecture and Ocean Engineering, Huazhong University of Science and Technology, Wuhan 430074, China
[b] Shenzhen Huazhong University of Science and Technology Research Institute, Shenzhen 518057, China
[c] Department of Robotics, CNRS-LIRMM-UMII, Montpellier Cedex 5 34095, France
[d] State Key Lab of Digital Manufacturing, Equipment and Technology, Huazhong University of Science and Technology, Wuhan 430074, China

ARTICLE INFO

Keywords:
Autonomous underwater vehicle (AUV)
Path following
Approach angle
Actuator saturation
Indirect adaptive fuzzy control

2020 MSC:
00-01
99-00

ABSTRACT

In this paper an approach-angle-based three-dimensional path-following control scheme has been proposed for underactuated Autonomous Underwater Vehicle (AUV) which experiences unknown actuator saturation and environmental disturbance. First, the path-following error dynamic model is derived based on the principle of relative motion which was followed by the design of approach-angle-based guidance law in both horizontal and vertical profiles of AUV to transform the three-dimensional tracking errors into heading angle and elevation angle tracking errors. The kinematic control law is designed based on the Lyapunov theory and backstepping technique. Second, the kinetic controller is designed based on the Lyapunov theory, backstepping technique and fuzzy logic system approximation method. The indirect adaptive fuzzy logic system is applied to approximate unknown smooth functions which are composed of coupled AUV hydrodynamics and complex differentials of desired pitch and yaw velocities. Moreover, the application of fuzzy control completely free from dependence on accurate AUV kinetic model. Considering a disturbance-like term, which is comprised of fuzzy logic system approximation error and bounded ocean disturbance, an adaptive law is designed to estimate the bound of it. Finally, two sets of comparative numerical simulations, including straight path following with different initial posture and spatial helix path following with sudden disturbance, are studied to illustrate the effectiveness and robustness of the proposed control scheme.

1. Introduction

Advancement in development of smart maneuvering marine vehicles offer scientists a large flexibility to conduct ocean exploration and exploitation (Chang et al., 2019; Lapierre and Soetanto, 2007). In particular, development of intelligent control system of marine vehicles greatly expands applicability in oceanic research (Cui et al., 2017; Peng et al., 2018; Yu et al., 2020; Zhang et al., 2018). A broad range of intelligent controllers has been proposed for the motion control of various types of marine vehicles such as Autonomous Underwater Vehicle (AUV), Remotely Operated Vehicle (ROV), Autonomous Surface Vehicle (ASV) and marine glider (Chu et al., 2019; Hussain et al., 2011; Mišković et al., 2016; Sun et al., 2014; Wang et al., 2021; Yu et al., 2017b). During the last decade, extensive research has been carried out to design marine vehicle motion controllers based on advanced methods which mainly include point stabilization, trajectory tracking and path-following methods. Among the said methods, path-following is considered a leading method in which a marine vehicle is forced to follow a reference spatial path and thus path-following and three-dimensional adaptive trajectory tracking are considered the most common methods for AUVs motion controllers (Chu et al., 2019; Shojaei, 2016) and underactuated stratospheric airships (Zuo et al., 2019). The actuator configuration of AUVs is designed according to the practical applications and typical underactuated configuration can satisfy the requirements of general scientific investigations such as high-speed-demanded applications (Chen and Zhu, 2019), scientific sampling and mapping (Sarda and Dhanak, 2019). Moreover, actuator configuration of the REMUS-100 AUV is considered classical in which the AUV is controlled with a main propeller, a pair of horizontal & vertical planes (cross-type stern rudders) which are placed on the tail

☆ Fully documented templates are available in the elsarticle package on CTAN.

* Corresponding author.
E-mail address: xbxiang@hust.edu.cn (X. Xiang).

https://doi.org/10.1016/j.apor.2020.102486
Received 1 June 2020; Received in revised form 3 November 2020; Accepted 8 December 2020
Available online 4 January 2021

side of the AUV (Sarda and Dhanak, 2019). Ocean exploration requires wide range of areas of research such as near-bottom sea search for which the AUVs are required to perform challenging maneuvers and navigate with better accuracy and efficiency. In order to meet these challenges, AUVs are to be designed accordingly such as Delphin 2 AUV and HURV (Xiang et al., 2020). Apart from typical actuator configuration, the MBARI AUV is actuated by an articulated ring wing and partially ducted thruster (Do and Pan, 2009; McEwen and Streitlien, 2001).

Fuzzy Control Adaptive fuzzy logic control methods mainly include direct adaptive fuzzy control and indirect adaptive fuzzy control. The former method aims to estimate and identify the unknown parts of the system model. Comparatively, the latter one is designed to approximate the unknown nonlinear terms and functions, hence to achieve Lyapunov stability (Peng et al., 2017; Yu et al., 2020). The indirect fuzzy logical system is allied to neural network systems in terms of unknown function approximation (Cui et al., 2017; Shojaei, 2016). Uncertainties and nonlinearities which includes uncertain parameters, uncertain dynamics and external interference are inevitable in a practical control system especially for marine vehicles with multiple uncertainties. Fuzzy logical control has shown great robustness and effectiveness for such uncertain nonlinear marine vehicles (Chu et al., 2019; Yu et al., 2020). In Liu et al. (2019), an adaptive semiglobally finite-time controller is designed for a class of uncertain strict-feedback nonlinear systems by using fuzzy logic control method, backstepping technique and prescribed performance function. It is proved that not only all states converge to a predefined zone in bounded time, but also all signals of the closed-loop systems are semiglobally finite-time stable. Besides, there are a variety of hybrid control methods which are composed of fuzzy logic control and conventional control methods, such as PID control (Chu et al., 2019; Tang et al., 2001), sliding mode control (Vijay and Jena, 2017), neural-networks control (Shojaei, 2016; Wang and Mendel, 1992) and so on.

Furthermore, swarm optimization is a solution for conventional fuzzy logic controllers to optimize optimal control parameters, such as Mamdani-type and Takagi-Sugeno-Kang. These new-type hybrid algorithms are implemented by optimizing some key parameters with different cost functions, which include the centers and the widths of the Gaussian membership functions in inputs and outputs. There are some applications of conventional fuzzy logical controller combining with Particle Swarm Optimization (PSO) (Bingül and Karahan, 2010; Nobile et al., 2018) and Grey Wolf Optimizer Algorithm (Precup et al., 2016) in multi-degree-of-freedom robots and manipulators. Since, there are a variety of derived algorithms for PSO are available therefore, PSO is considered one of the most effective and succinct solutions for nonlinear, high-dimensional and complex problems. Moreover, PSO is also utilized on multi-input and multi-output control systems. In Bingül and Karahan (2010), 60 parameters in 15 membership functions and 25 fuzzy rules are optimized by PSO to control 1 manipulator joint. However, for the swarm optimization method, mature stability analysis and theory to guarantee the control system stability is lacking.

Guidance Law There are several nice properties of traditional Line-Of-Sight (LOS) guidance law. Since, the LOS guidance law can synthesize the cross-tracking error and heading error into a virtual control variable and thus widely being used in two-dimensional and three-dimensional path following and trajectory tracking of underactuated marine vehicles (Chu et al., 2019; Shojaei, 2016; Yu et al., 2018). It is highlighter in Borhaug and Pavlov (2008) that conventional LOS guidance law has the drawback of being susceptible to environmental disturbances in the kinematic level. Whereas, Integral LOS (ILOS) is proposed to compensate for the irrotational and constant ocean currents (Borhaug and Pavlov, 2008). The concept of approach angle, as another kinematic guidance law, was proposed on a unicycle-type and two-steering wheels mobile robots in 1993 (Alain and Claude, 1993) and subsequently, it was also implemented on a horizontal path following control of an under-actuated AUV (Lapierre and Soetanto, 2007). In Wang and Ahn (2019), a hyperbolic-tangent guidance law is designed to guide the heading angle for an underactuated vehicle, by defining a virtually desired sideslip angle of which the tangent-nonlinearity is exactly identified by a finite-time sideslip observer.

Actuator saturation Saturation is a nonlinear response and common physical constraint for all realizable actuators and sensors. This is considered to be a major nonlinearity of conventional actuators such as main propeller and control fins. Hence, actuator saturation is extensively studied in the robotsmotion control which includes, point stabilization, path following and trajectory tracking (Cui et al., 2016; Wang et al., 2017b; Zheng and Sun, 2015). The research study on actuator saturation can be bifurcated as nonlinearity compensation and saturated-function approximation. Literature survey reveals that, the logistic sigmoid function and the hyperbolic tangent function (tanh) are commonly used for saturation approximation which makes smooth functions differentiable along the solution (Xu et al., 2016). In Zheng and Sun (2015), the *tanh* function is applied to approximate the non-differentiable actuator saturation function. Whereas, the difference between *tanh* function and physical saturation is bounded which facilitates the application of the back-stepping technique. In Shojaei (2016) and Yu et al. (2018), actuator saturation nonlinearity is compensated with fuzzy logic systems and neural networks, respectively.

The contribution of this work is three-fold:

(1) The path-following error dynamics is derived based on the theory of relative velocity, which simplifies the direct differential on tracking errors (Breivik and Fossen, 2005; Yu et al., 2020), and avoids potential singularities caused by inverse trigonometric calculation such as *arcsin* function (Yu et al., 2017a). Further, the relative velocity-based deduction gets out of the complex coordinates' transformation (Breivik and Fossen, 2005).
(2) Fuzzy logic system is adopted to approximate coupled kinetic model and high-order differential function. Particularly, the proposed scheme completely free from dependence on accurate kinetic model. Comparatively, most of fuzzy control and neural network-based tracking control schemes are designed based on partially known model parameters (Liu et al., 2016; Zheng et al., 2018; Zheng and Sun, 2015).
(3) A novel saturated kinetic control scheme is proposed by considering unknown bound of actuator saturation. In contrast, the known saturation bound is required for saturated function approximation (Chu et al., 2019; Xu et al., 2016; Zheng and Sun, 2015) and saturated truncation estimation (Shojaei, 2016; Yu et al., 2020; 2018). Further, the bound of disturbance-like term is compensated so that tracking errors can converge to zero.

The rest of this paper is organized as follows: In Section 2, control preliminaries, notations and assumptions are introduced. Further, under-actuated AUV kinematic and kinetic models, path-following-related mission and actuator saturation are stated and formulated. In Section 3, the path-following error model is derived and the kinematic approach-angle-based guidance law is designed. The kinematic and kinetic controllers are designed based on the Lyapunov theory, backstepping technique. Particularly, the indirect adaptive fuzzy logic system approximation technique is utilized to approximate unknown functions. Section 4 provides two sets of comparative numerical simulations. Conclusion remarks are summarized in Section 5.

2. Preliminaries and problem formulation

Initially, some control preliminaries and notations are described in this section. Afterwards, kinematic and kinetic equations of under-actuated AUVs are derived. Finally, actuator saturation, path-following mission, control objectives and some assumptions are summarized and formulated in this section.

Table 1
Notations for 3 frames.

Frames	Origin	Notation	Description
$\{NED\}$	Arbitrary	$\{I\}$	Earth-fixed inertial frame (North-East-Down)
$\{uvw\}$	O_b	$\{B\}$	Body-fixed fame
$\{x_{SF}y_{SF}z_{SF}\}$	O_p	$\{F\}$	Serret-Frenet frame

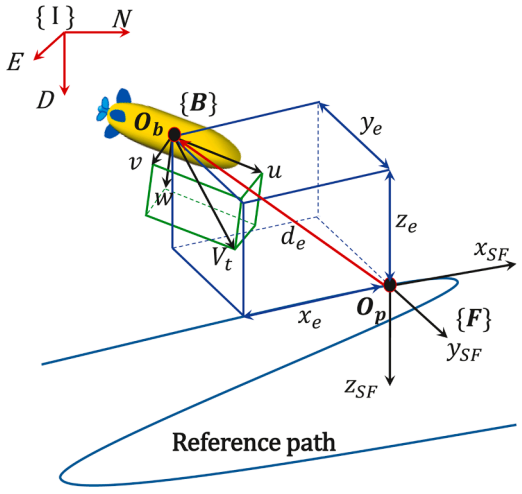

Fig. 1. Geometric illustration of three-dimensional path following with an an underactuated AUV.

2.1. Preliminaries and notations

The conventional fuzzy logic system, including Takagi-Sugeno-Kang (TSK) (Takagi and Sugeno, 1985) and Mamdani (H and Sedrak, 1993), is composed of fuzzification, fuzzy inference, and defuzzification. Herein, the inputs of the conventional fuzzy logic controller usually include error e and the differential $\dot{e}$. The output of the fuzzy logic system can be directly distributed to actuators, which is similar to the PID controller. Moreover, the commonly used IF-THEN rules which are developed from empirical knowledge can be described in the following way:

$$R^i: \text{IF } e \text{ is } F_e^i, \text{THEN } u \text{ is } \varpi_i \tag{1}$$

where F_e^i are input fuzzy sets, and $\varpi_i (i = 1, 2, \cdots, n)$ are output fuzzy singletons. The conventional fuzzy logic controller is composed of a fixed number of IF-THEN rules and predefined membership functions, which is vulnerable for complicated, time-varying, strong coupling, and nonlinear systems.

To facilitate the path-following control scheme design, two lemmas can be described herein.

Lemma 1. *(Universal approximation theorem of fuzzy basis functions) (Wang and Mendel, 1992) If an unknown continuous function $f(x)$ is defined on a compact set Ω whose analytic expression is unknown, then there exists a fuzzy logic system $\boldsymbol{\xi}^T \boldsymbol{S}(x)$ such that*

$$\sup_{x\in\Omega} \left| f(x) - \boldsymbol{\xi}^T \boldsymbol{S}(x) \right| \le \epsilon \tag{2}$$

where the fuzzy logic system approximation error $\epsilon > 0$, $\boldsymbol{\xi}^T = [\xi_1, \xi_2, \cdots, \xi_n]^T$ is the idea weight vector. $\boldsymbol{S}(x)$ and $s_i(x)$ are the basis function vector and Gaussian function respectively, which can be formulated in the following way:

$$\boldsymbol{S}(x) = \frac{[s_1(x), s_2(x), \cdots, s_N(x)]^2}{\Sigma_{i=1}^N s_i(x)} \tag{3}$$

$$s_i(x) = \exp\left[\frac{-(x-\kappa_i)^T (x-\kappa_i)}{\eta_i^T \eta_i}\right] \qquad (i = 1, 2, \cdots, N) \tag{4}$$

where N is the number of fuzzy rules, $\kappa_i = [\kappa_{i1}, \kappa_{i2}, \cdots, \kappa_{iN}]^T$ is the center vector, $\eta_i = [\eta_{i1}, \eta_{i2}, \cdots, \eta_{iN}]^T$ is the width vector of Gaussian functions (Liu et al., 2019).

Lemma 2. *(Barbalat's lemma) (Popov and Georgescu, 1973; Slotine and Li, 1991) Consider a function $f(t): \mathbb{R}^+ \to \mathbb{R}$. If $f(t)$ is differentiable and $\lim_{t\to\infty} \int_0^\tau f(t)dt$ exist and is bounded, then $\lim_{t\to\infty} f(t) = 0$.*

2.2. Problem formulation

To describe the AUVs motion in different coordinate frames, let us define some notations utilized in this paper as listed in Tab. 1 and shown in Fig. 1.

In the $\{NED\}$ frame, the kinematic and kinetic equation of an underactuated AUV can be modeled as follows:

$$\begin{cases} \dot{\boldsymbol{\eta}} = \boldsymbol{R}\boldsymbol{\nu} \\ \boldsymbol{M}\dot{\boldsymbol{\nu}} + \boldsymbol{C}\boldsymbol{\nu} + \boldsymbol{D}\boldsymbol{\nu} + \boldsymbol{g}(\boldsymbol{\nu}) = \boldsymbol{\tau} + \boldsymbol{\tau}_d \end{cases} \tag{5}$$

with the matrix

$$\boldsymbol{R}(\boldsymbol{\nu}) = \begin{pmatrix} \cos\theta\cos\psi & -\sin\psi & \sin\theta\cos\psi & 0 & 0 \\ \cos\theta\sin\psi & \cos\psi & \sin\theta\sin\psi & 0 & 0 \\ -\sin\theta & 0 & \cos\theta & 0 & 0 \\ 0 & 0 & 0 & 1 & 0 \\ 0 & 0 & 0 & 0 & 1/\cos\theta \end{pmatrix} \tag{6}$$

where the location and velocity vector are given as $\boldsymbol{\eta} = [x, y, z, \theta, \psi]^T$ and $\boldsymbol{\nu} = [u, v, w, q, r]^T$, which are locations, angles and velocities on surge, sway, heave, pitch and yaw directions respectively. $\boldsymbol{M}$, $\boldsymbol{C}$ and $\boldsymbol{D}$ denote inertia, Coriolis and damping matrixes respectively. The vector $\boldsymbol{g}(\boldsymbol{\nu})$ represent generalized gravitational and buoyancy forces.

Furthermore, the kinetic equation can be rewritten in differential form Do and Pan (2009)

$$\begin{cases} \dot{u} &= \dfrac{m_{22}vr + m_{33}wq - d_{11}u + \tau_{du} + sat(\tau_u)}{m_{11}} \\ \dot{v} &= \dfrac{m_{11}ur - d_{22}v + \tau_{dv}}{m_{22}} \\ \dot{w} &= \dfrac{m_{11}uq - d_{33}w + \tau_{dw}}{m_{33}} \\ \dot{q} &= \dfrac{(m_{33} - m_{11})uw - d_{55}q - Gh\sin\theta + \tau_{dq} + sat(\tau_q)}{m_{55}} \\ \dot{r} &= \dfrac{(m_{11} + m_{22})uv - d_{66}r + \tau_{dr} + sat(\tau_r)}{m_{66}} \end{cases} \tag{7}$$

where $m_{(\cdot)}$ and $d_{(\cdot)}$ denote the inertial and hydrodynamic damping coefficients respectively. τ_u, τ_q and τ_r are control force and moments from main propeller and stern control surfaces, respectively. τ_{du}, τ_{dv}, τ_{dw}, τ_{dq} and τ_{dr} are forces and moments caused by oceanic disturbance on surge, sway, heave, pitch and yaw directions respectively. The input saturation function $sat(x)$ will be detailed later.

The kinetic equations of AUV in actuated freedom can be rewritten as follows:

$$\begin{cases} \dot{u} &= f_u + g_u\tau_u + d_{u1} \\ \dot{q} &= f_q + g_q\tau_q + d_{q1} \\ \dot{r} &= f_r + g_r\tau_r + d_{r1} \end{cases} \tag{8}$$

where f_u, f_q and f_r are unknown smooth functions depending on AUVs hydrodynamics. And parameters g_u, g_q and g_r are unknown constants. Smooth unknown functions d_{u1}, d_{q1} and d_{r1} are disturbances-like terms, which include external disturbance, unmodeled dynamics.

The control force saturation for propeller and control surfaces can be

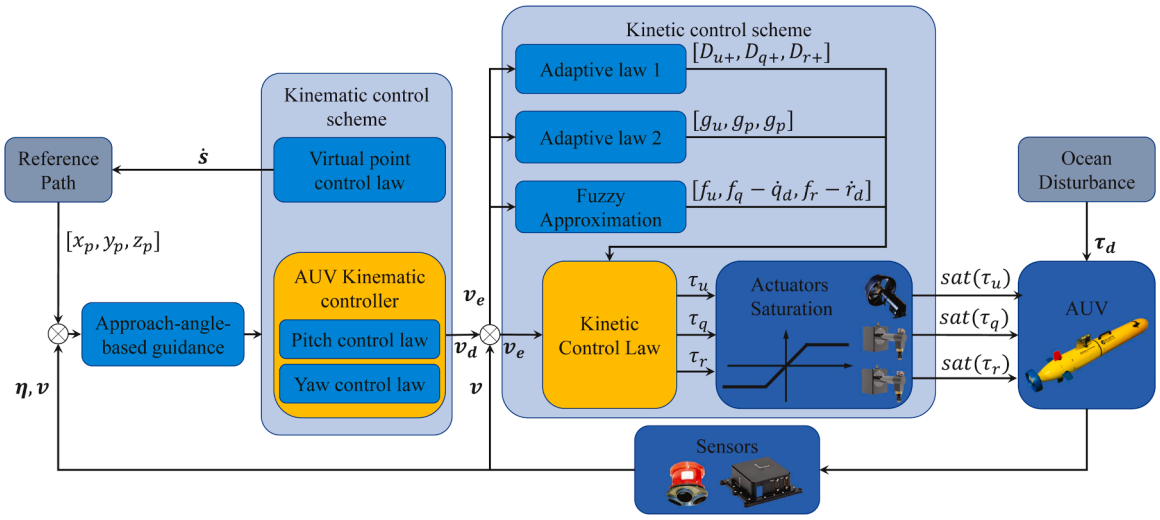

Fig. 2. Saturated path-following control block diagram for underactuated AUVs.

formulated as:

$$\tau_{input} = sat(\tau) = \begin{cases} \tau_{max} & \tau_{max} < \tau \\ \tau & \tau_{min} \le \tau \le \tau_{max} \\ \tau_{min} & \tau < \tau_{min} \end{cases} \tag{9}$$

with $\tau = \tau_u, \tau_q$ and τ_r. And τ_{max} and τ_{min} denote the upper and lower bounds of control forces respectively (Naik and Singh, 2007; Zheng et al., 2018).

Let us define a parameterized reference path which is propagated based on the variable $\varpi(t)$, and the virtual tracking point on the path in $\{NED\}$ frame is denoted with $\boldsymbol{O_p}(x_p, y_p, z_p)$. By defining a coordinate frame whose origin is located at $\boldsymbol{O_p}$, the route angle at point $\boldsymbol{O_p}$ can be denoted in the following way:

$$\begin{cases} \psi_p = atan2\left(\dot{y}_p, \dot{x}_p\right) \\ \theta_p = \arctan\left(\dfrac{-\dot{z}_p}{\sqrt{\dot{x}_p^2 + \dot{y}_p^2}}\right) \end{cases} \tag{10}$$

with $\dot{x}_p = dx_p/d\varpi$, $\dot{y}_p = dy_p/d\varpi$ and $\dot{z}_p = dz_p/d\varpi$. Furthermore, the velocity of $\boldsymbol{O_p}$ can be denoted as $u_p = \sqrt{\dot{x}_p^2 + \dot{y}_p^2 + \dot{z}_p^2}$. The vectorial difference between the AUV and the virtual point $\boldsymbol{O_p}$ can be denoted as:

$$\boldsymbol{d_e} = \begin{pmatrix} x_e \\ y_e \\ z_e \end{pmatrix} = \boldsymbol{R}_z(\psi_p)\boldsymbol{R}_y(\theta_p) \begin{pmatrix} x - x_p \\ y - y_p \\ z - z_p \end{pmatrix} \tag{11}$$

with rotation matrix $\boldsymbol{R}_z(\psi_p) = (c\psi_p, -s\psi_p, 0; s\psi_p, c\psi_p, 0; 0, 0, 1)$ and $\boldsymbol{R}_y(\theta_p) = (c\theta_p, s\theta_p, 0; 0, 1, 0; -s\theta_p, 0, c\theta_p)$, where $c\Delta := \cos\Delta$ and $s\Delta := \sin\Delta$ with $\Delta = \theta_p, \psi_p$.

Hence, the path-following control objectives can be formulated as:

$$\begin{cases} \lim\limits_{t\to\infty} \boldsymbol{d_e} = \boldsymbol{0} \\ \lim\limits_{t\to\infty} (\psi_v, \theta_v) = (\psi_p, \theta_p) \end{cases} \tag{12}$$

with angles $\theta_v = \theta - \alpha$ and $\psi_v = \psi - \beta$. The angle of attack and sideslip angle are given as $\alpha = \arctan(-w/u)$ and $\beta = \arctan(v/\sqrt{u^2 + w^2})$.

The assumptions taken into consideration are summarized as under:

(1) The reference path is smooth so that the parameterized path in x, y, and z directions are differentiable. The path curvature c_1 and path torsion c_2 is continued.
(2) The disturbances-like terms are bounded with unknown constant bounds $\boldsymbol{D} > \boldsymbol{0}$, $\boldsymbol{D} = [D_u, D_v, D_w, D_q, D_r]^T$, namely $|d_u| < D_u$, $|d_v| < D_v$, $|d_w| < D_w$, $|d_q| < D_q$ and $|d_r| < D_r$ (Qiao et al., 2017; Wang et al., 2017a).
(3) The unknown functions f_u, f_q and f_r are smooth, such that it can be approximated by fuzzy basis functions.
(4) For the universal approximation of fuzzy logic system, the idea weight $\boldsymbol{W}^*$ is bounded. The approximation error is bounded with unknown bound $D_\varepsilon > 0$, namely $|\varepsilon(x)| \le D_\varepsilon$.

Above assumptions are reasonable since AUV hydrodynamic coefficients and velocity states are continued. Practically, there are many path planning and smoothing methods which can provide continued path curvature and torsion, such as B-spline and Fermats spiral. In addition, the oceanic disturbance are bounded in practice even though the bounds are unknown.

3. Controller Design

In this section, a successive three-dimensional path following guidance law and control schemes have be designed for the underactuated AUVs. The control block diagram for AUV path following is designed as shown in Fig. 2. The approach-angle-based guidance law is designed for the three-dimensional path-following mission. Kinematic control schemes for virtual tracking point and AUV velocities, are designed by using the backstepping technique and Lyapunov theory to guarantee the stability of the kinematic loop. Kinetic control scheme is designed based on the indirect adaptive fuzzy logic system and adaptive compensation control laws in the presence of actuators saturation.

3.1. Kinematic Controller

The theory of relative motion also known as the velocity composition theorem, can be denoted as follows:

$$\boldsymbol{v}_a = \boldsymbol{v}_e + \boldsymbol{v}_r \tag{13}$$

where $\boldsymbol{v}_a$, $\boldsymbol{v}_e$ and $\boldsymbol{v}_r$ denote the vectorial absolute velocity, relative velocity and transportation velocity respectively of a relative-moving particle.

Based on the definition of the coordinate frames in Tab. 1 and Fig. 1, the absolute velocity of the AUV in $\{NED\}$ frame can be denoted as:

$$\left(\frac{d\boldsymbol{O_b}}{dt}\right)_I = \left(\frac{d\boldsymbol{O_p}}{dt}\right)_I + \left({}^F_I R\right)^{-1}\left(\left(\frac{d\boldsymbol{d}}{dt}\right)_F + (\boldsymbol{w_F} \otimes \boldsymbol{d})\right) \tag{14}$$

where the rotation matrix ${}^F_I\boldsymbol{R}$ represents the transformation from frame $\{I\}$ to frame $\{F\}$, which can be derived in the following way:

$${}^F_I\boldsymbol{R} = \boldsymbol{R}_{O_p,z}(\psi_p)\boldsymbol{R}_{O_p,y}(\theta_p) \tag{15}$$

As shown in Fig. 1, the vectorial velocity of the tracking error $\boldsymbol{d_e}$ can be derived in the following way:

$$\left(\frac{d\boldsymbol{d_e}}{dt}\right)_I = \left(\frac{d\boldsymbol{O_b}}{dt}\right)_I - \left(\frac{d\boldsymbol{O_p}}{dt}\right)_I \tag{16}$$

Hence, the transportation motion equation can be rewritten as:

$${}^F_I\boldsymbol{R}\left(\frac{d\boldsymbol{O_b}}{dt}\right)_I = \left(\frac{d\boldsymbol{O_p}}{dt}\right)_F + \left(\frac{d\boldsymbol{d_e}}{dt}\right)_F + (\boldsymbol{w_F} \otimes \boldsymbol{d_e}) \tag{17}$$

with $\left(\frac{d\boldsymbol{O_b}}{dt}\right)_I = (\dot{x}, \dot{y}, \dot{z})^T$, $\left(\frac{d\boldsymbol{O_p}}{dt}\right)_F = (\dot{s}, 0, 0)^T$ and $\left(\frac{d\boldsymbol{d_e}}{dt}\right)_F = (\dot{x}_e, \dot{y}_e, \dot{z}_e)^T$.

$$\boldsymbol{w_F} \otimes \boldsymbol{d_e} = \begin{pmatrix} 0 \\ c_2\dot{s} \\ c_1\dot{s} \end{pmatrix} \otimes \begin{pmatrix} x_e \\ y_e \\ z_e \end{pmatrix} = \begin{pmatrix} c_2\dot{s}z_e - c_1\dot{s}y_e \\ c_1\dot{s}x_e \\ -c_2\dot{s}x_e \end{pmatrix}$$

where c_1 and c_2 are curvature and torsion of the reference path in $\boldsymbol{O_p}$ respectively. Besides, s is the signed curvilinear abscissa of $\boldsymbol{O_P}$ such that $ds/dt = u_p$. The relative velocity of $\boldsymbol{O_b}$ can be deduced based on the known path parameters, that is

$$\begin{aligned}\left(\frac{d\boldsymbol{O_b}}{dt}\right)_F &= {}^F_I\boldsymbol{R}(\psi_p, \theta_p)\cdot{}^I_B\boldsymbol{R}(\psi, \theta)\cdot(u, v, w)^T \\ &= \boldsymbol{R}_{O_B,z}(\psi_e)\cdot\boldsymbol{R}_{O_B,y}(\theta_e)\cdot(\nu_t, 0, 0)^T \\ &= \begin{pmatrix} \cos(\psi_e)\cos(\theta_e)\nu_t \\ \sin(\psi_e)\cos(\theta_e)\nu_t \\ -\sin(\theta_e)\nu_t \end{pmatrix}\end{aligned} \tag{18}$$

with resultant velocity $\nu_t = \sqrt{u^2 + v^2 + w^2} > 0$.

Based on the above deduction, the differential of the vectorial tracking error can be derived in the following way:

$$\left(\frac{d\boldsymbol{d_e}}{dt}\right)_F = \begin{pmatrix} \cos(\psi_e)\cos(\theta_e)\nu_t - (c_2z_e - c_1y_e + 1)\dot{s} \\ \sin(\psi_e)\cos(\theta_e)\nu_t - c_1x_e\dot{s} \\ -\sin(\theta_e)\nu_t + c_2x_e\dot{s} \end{pmatrix} \tag{19}$$

Furthermore, based on the above definition, the differential of tracking angles can be derived as follows:

$$\begin{cases} \dot{\psi}_e &= r/\cos(\theta) + \dot{\beta} - c_1\dot{s} \\ \dot{\theta}_e &= q + \dot{\alpha} - c_2\dot{s} \end{cases} \tag{20}$$

Then design the approach-angle-based guidance law as:

$$\begin{cases} \psi_{app} = -\psi_a\dfrac{e^{k_\psi y_e} - 1}{e^{k_\psi y_e} + 1} \\ \theta_{app} = \theta_a\dfrac{e^{k_\theta z_e} - 1}{e^{k_\theta z_e} + 1} \end{cases} \tag{21}$$

where $\psi_a \in (0, \pi/2)$ and $\theta_a \in (0, \pi/2)$ are constant maximum yaw and pitch guidance angles, respectively.

Then design the kinematic control scheme for the virtual point and AUVs velocities as:

$$\begin{cases} \dot{\varpi} &= \dfrac{-\nu_t\cos(\psi_e)\cos(\theta_e) + k_1x_e}{\sqrt{\dot{x}_p^2 + \dot{y}_p^2 + \dot{z}_p^2}} \\ q_d &= -\dot{\alpha} + c_2\dot{s} + \dot{\theta}_{app} - k_2(\theta_e - \theta_{app}) + z_e v_t f(\theta_e, \theta_{app}) \\ r_d &= \cos\theta\Big(-\dot{\beta} + c_1\dot{s} + \dot{\psi}_{app} - k_3(\psi_e - \psi_{app}) - y_e v_t f(\psi_e, \psi_{app})\Big) \end{cases} \tag{22}$$

where $\dot{s} = \sqrt{\dot{x}_p^2 + \dot{y}_p^2 + \dot{z}_p^2}$. The function $f(a,b) = \frac{\sin a - \sin b}{a - b}$. It is noted that the function $f(a,b)$ is non-singular around $(a \to b)$ due to that

$$\lim_{a\to b}\frac{\sin a - \sin b}{a - b} \overset{\nabla = a-b}{=\!=\!=} \lim_{\nabla\to 0}\frac{\sin a - \sin(a - \nabla)}{\nabla} = \cos a \tag{23}$$

3.2. Kinetic Controller

By recalling the saturation function in (9) and simplified AUV kinetic model in (8), the AUV kinetic equations in actuated profiles can be rewritten as follows:

$$\begin{cases} \dot{u} &= f_u + g_u sat(\tau_u) + d_u \\ \dot{q} &= f_q + g_q sat(\tau_q) + d_q \\ \dot{r} &= f_r + g_r sat(\tau_r) + d_r \end{cases} \tag{24}$$

Let us define the kinetic tracking errors as $u_e = u - u_d$, $q_e = q - q_d$ and $r_e = r - r_d$, where desired pitch velocity q_d and yaw velocity r_d have been designed in (22), and the desired travelling surge velocity u_d is given constant or known time-varying regularity.

Considering the kinetic velocity tracking errors, choose a positive function in the following way:

$$V_2 = \frac{1}{2}(u_e^2 + q_e^2 + r_e^2) \tag{25}$$

By recalling the kinematic model in (24) and definition on velocity tracking errors u_e, q_e & r_e, the differential of V_2 can be derived as:

$$\begin{aligned}\dot{V}_2 &= u_e\Big(f_u + g_u sat(\tau_u) + d_u - \dot{u}_d\Big) + \\ &\quad q_e\Big(f_q + g_q sat(\tau_q) + d_q - \dot{q}_d\Big) + \\ &\quad r_e\Big(f_r + g_r sat(\tau_r) + d_r - \dot{r}_d\Big) \\ &= u_e\Big(f_u - \dot{u}_d\Big) + q_e\Big(f_q - \dot{q}_d\Big) + r_e\Big(f_r - \dot{r}_d\Big) + u_e d_u + \\ &\quad q_e d_q + r_e d_r + u_e g_u sat(\tau_u) + q_e g_q sat(\tau_q) + r_e g_r sat(\tau_r)\end{aligned} \tag{26}$$

According to the kinematic control law in (22), we have that $\dot{q}_d$ and $\dot{r}_d$ are continuous and differentiable. For an AUV traveling with constant surge velocity, we have that $\dot{u}_d = 0$. Hence, by recalling the assumption (3) and Lemma 1, the fuzzy logic basis functions can be utilized herein to approximate functions (f_u), $(f_q - \dot{q}_d)$ and $(f_r - \dot{r}_d)$, which can be formulated as follows:

$$\begin{cases} f_u' &= f_u = \boldsymbol{\xi_u}\boldsymbol{S_u} + \varepsilon_u \\ f_q' &= f_q - \dot{q}_d = \boldsymbol{\xi_q}\boldsymbol{S_q} + \varepsilon_q \\ f_r' &= f_r - \dot{r}_d = \boldsymbol{\xi_r}\boldsymbol{S_r} + \varepsilon_r \end{cases} \tag{27}$$

By substituting (27) into (26), it can be deduced as follows:

$$\begin{aligned}\dot{V}_2 &= u_e\boldsymbol{\xi_u}\boldsymbol{S_u} + q_e\boldsymbol{\xi_q}\boldsymbol{S_q} + r_e\boldsymbol{\xi_r}\boldsymbol{S_r} + \\ &\quad u_e(d_u + \varepsilon_u) + q_e(d_q + \varepsilon_q) + r_e(d_r + \varepsilon_r) + \\ &\quad u_e g_u sat(\tau_u) + q_e g_q sat(\tau_q) + r_e g_r sat(\tau_r)\end{aligned} \tag{28}$$

According to *Assumption 2* and *4*, we have $d_u + \varepsilon_u \le D_{u+}$ with $D_{u+} = D_u + D_{ue}$. Furthermore, the similar conclusion can be derived in pitch and yaw directions: $d_q + \varepsilon_q \le D_{q+}$ and $d_r + \varepsilon_r \le D_{r+}$. It is noted that terms D_{u+}, D_{q+} and D_{r+} are unknown due to the fact that bounds of disturbance and approximation errors are unknown and unmeasurable. Let us define the parameter approximation errors as

$$\begin{cases} \tilde{\boldsymbol{\xi}}_\nabla = \hat{\boldsymbol{\xi}}_\nabla - \boldsymbol{\xi}_\nabla \\ \tilde{D}_{\nabla+} = \hat{D}_{\nabla+} - D_{\nabla+} - g_\nabla \\ \tilde{g}_\nabla = \bar{g}_\nabla \end{cases} \tag{29}$$

with $\nabla = u, q, r$ and $\bar{g}_\nabla = 1/\hat{g}_\nabla$.

Design the kinetic control scheme in the following way:

$$\begin{cases} \tau_u &= -sign(u_e)\bar{\tau}_u\left(1+\hat{g}_u\right) \\ \tau_q &= -sign(q_e)\bar{\tau}_q\left(1+\hat{g}_q\right) \\ \tau_r &= -sign(r_e)\bar{\tau}_r\left(1+\hat{g}_r\right) \end{cases} \tag{30}$$

with

$$\begin{cases} \bar{\tau}_u &= |\hat{\boldsymbol{\xi}}_{\boldsymbol{u}}\boldsymbol{S}_{\boldsymbol{u}}| + \hat{D}_{u+} + k_4|u_e| \\ \bar{\tau}_q &= |\hat{\boldsymbol{\xi}}_{\boldsymbol{q}}\boldsymbol{S}_{\boldsymbol{q}}| + \hat{D}_{q+} + k_5|q_e| \\ \bar{\tau}_r &= |\hat{\boldsymbol{\xi}}_{\boldsymbol{r}}\boldsymbol{S}_{\boldsymbol{r}}| + \hat{D}_{r+} + k_6|r_e| \end{cases} \tag{31}$$

and adaptive update law for control parameters is given as:

$$\begin{cases} \dot{\hat{g}}_\nabla = \zeta_{g\nabla}\hat{g}_\nabla^3|\nabla_e|\bar{\tau}_\nabla \\ \dot{\hat{D}}_{\nabla+} = \zeta_{D\nabla}|\nabla_e| \\ \dot{\hat{\boldsymbol{\xi}}}_\nabla = \zeta_{\xi\nabla}\nabla_e\boldsymbol{S}_\nabla \end{cases} \tag{32}$$

where k_4, k_5 and k_6 are positive constants. $\zeta_{g\Delta}$, $\zeta_{D\Delta}$ and $\zeta_{\xi\Delta}$ are positive adaptive constants.

3.3. Stability analysis

Theorem 1. *The approach angle based guidance law given by (21) and kinematic control scheme given by (22) render the state* $(x_e, y_e, z_e, (\theta_e - \theta_{app}), (\psi_e - \psi_{app})) = (0,0,0,0,0)$ *globally uniformly asymptotically stable.*

Proof. Choose a candidate Lyapunov function as follows:

$$V_1 = \frac{1}{2}\left(x_e^2 + y_e^2 + z_e^2 + \left(\theta_e - \theta_{app}\right)^2 + \left(\psi_e - \psi_{app}\right)^2\right) \tag{33}$$

.

Based on the deduction of tracking error dynamics in (19,20), then the differential of V_1 can be derived as follows:

$$\begin{aligned} \dot{V}_1 &= x_e\dot{x}_e + y_e\dot{y}_e + z_e\dot{z}_e + \left(\theta_e - \theta_{app}\right)\left(\dot{\theta}_e - \dot{\theta}_{app}\right) + \left(\psi_e - \psi_{app}\right)\left(\dot{\psi}_e - \dot{\psi}_{app}\right) \\ &= x_e(\cos\psi_e\cos\theta_e v_t - (c_2 z_e - c_1 y_e + 1)\dot{s}) + \\ &\quad y_e(\sin\psi_e\cos\theta_e v_t - c_1 x_e\dot{s}) + z_e(-\sin\theta_e v_t + c_2 x_e\dot{s}) + \\ &\quad \left(\theta_e - \theta_{app}\right)\left(q + \dot{\alpha} - c_2\dot{s} - \dot{\theta}_{app}\right) + \\ &\quad \left(\psi_e - \psi_{app}\right)\left(r/\cos\theta + \dot{\beta} - c_1\dot{s} - \dot{\psi}_{app}\right) \end{aligned} \tag{34}$$

Then by substituting kinematic controller (22) into (34), we have that

$$\begin{aligned} \dot{V}_1 &= x_e(v_t\cos\psi_e\cos\theta_e - \dot{s}) + y_e v_t\sin\psi_e\cos\theta_e - z_e v_t\sin\theta_e + \\ &\quad \left(\theta_e - \theta_{app}\right)\left(q + \dot{\alpha} - c_2\dot{s} - \dot{\theta}_{app}\right) + \left(\psi_e - \psi_{app}\right)\left(r/\cos\theta + \dot{\beta} - c_1\dot{s} - \dot{\psi}_{app}\right) \\ &= -k_1 x_e^2 - k_2\left(\theta_e - \theta_{app}\right)^2 - k_3\left(\psi_e - \psi_{app}\right)^2 + y_e v_t\sin\psi_{app} - z_e v_t\sin\theta_{app} \\ &\le 0 \end{aligned} \tag{35}$$

According to the approach angles in (21), we have $y_e\sin\psi_{app} \le 0$, $\forall [y_e, \psi_{app}] \in \mathbb{R}^2$, and $z_e\sin\theta_{app} \ge 0$, $\forall [z_e, \theta_{app}] \in \mathbb{R}^2$. Besides, the resultant velocity of the vehicle $v_t > 0$. Since $\dot{V}_1 \le 0$, and V_1 is a positive and monotonically decreasing function, $\lim_{t\to\infty} V_1$ exists. Then by recalling the Barbalat's lemma, it can be concluded that $\lim_{t\to\infty}\dot{V}_1 = 0$. Hence the related path-following errors are bounded and asymptotically converge to the invariant set. Hence, it can be concluded that $\lim_{t\to\infty} V_1 = 0$, namely $x_e = 0$, $y_e = 0$, $z_e = 0$, $\psi_e \to \psi_{app} \to 0$ and $\theta_e \to \theta_{app} \to 0$. Thus it can be proved that the kinematic system in (5) is asymptotically stable under the guidance law (21) and control law (22). □

Theorem 2. *Consider an underactuated AUV with kinematic and kinetic models as shown in (5, 24). Guidance law (21), kinematic control law (22), and kinetic control law (30) with parameter update law (31, 32) render kinematic and kinetic tracking errors converge to zero.*

Proof. Considering the kinematic tracking errors, kinetic velocity tracking errors, and system approximation errors, construct the following candidate Lyapunov function:

$$V_3 = V_1 + V_2 + \sum_{i=u,q,r}\left(\frac{\tilde{g}_i^2}{\zeta_{gi}} + \frac{\tilde{D}_{i+}^2}{\zeta_{Di}} + \frac{\tilde{\boldsymbol{\xi}}_i^T\tilde{\boldsymbol{\xi}}_i}{\zeta_{\xi i}}\right) \tag{36}$$

Based on the deduction on V_1 and V_2 in (35) and (26), and by recalling the definition on control parameters in (29), the differential of V_3 can be derived as follows:

$$\begin{aligned} \dot{V}_3 &= \dot{V}_1 + \dot{V}_2 + \sum_{i=u,q,r}\left(\frac{\tilde{g}_i\dot{\tilde{g}}_i}{\zeta_{gi}} + \frac{\tilde{D}_{i+}\dot{\hat{D}}_{i+}}{\zeta_{Di}} + \frac{\tilde{\boldsymbol{\xi}}_i^T\dot{\hat{\boldsymbol{\xi}}}_i}{\zeta_{\xi i}}\right) \\ &= -k_1 x_e^2 - k_2\left(\theta_e - \theta_{app}\right)^2 - k_3\left(\psi_e - \psi_{app}\right)^2 + y_e v_t\sin\psi_{app} - z_e v_t\sin\theta_{app} \\ &\quad + u_e\left(f_u - \dot{u}_d\right) + q_e\left(f_q - \dot{q}_d\right) + r_e\left(f_r - \dot{r}_d\right) + u_e d_u + q_e d_q + r_e d_r \\ &\quad + u_e g_u sat(\tau_u) + q_e g_q sat(\tau_q) + r_e g_r sat(\tau_r) \\ &\quad + \sum_{i=u,q,r}\left(\frac{\tilde{g}_i\dot{\tilde{g}}_i}{\zeta_{gi}} + \frac{\tilde{D}_{i+}\dot{\hat{D}}_{i+}}{\zeta_{Di}} + \frac{\tilde{\boldsymbol{\xi}}_i^T\dot{\hat{\boldsymbol{\xi}}}_i}{\zeta_{\xi i}}\right) \end{aligned} \tag{37}$$

Then by recalling the fuzzy logical basis functions approximation in (27) and definition on parameter approximation errors in (29), (37) can be deduced as follows:

$$\begin{aligned}\dot{V}_3 &= -k_1x_e^2 - k_2\left(\theta_e-\theta_{app}\right)^2 - k_3\left(\psi_e-\psi_{app}\right)^2 + y_ev_t\sin\psi_{app} - z_ev_t\sin\theta_{app} + \\ &\quad u_e\boldsymbol{\xi}_{\boldsymbol{u}}\boldsymbol{S}_{\boldsymbol{u}} + q_e\boldsymbol{\xi}_{\boldsymbol{q}}\boldsymbol{S}_{\boldsymbol{q}} + r_e\boldsymbol{\xi}_{\boldsymbol{r}}\boldsymbol{S}_{\boldsymbol{r}} + u_e\left(d_u+\varepsilon_u\right) + q_e\left(d_q+\varepsilon_q\right) + r_e\left(d_r+\varepsilon_r\right) + \\ &\quad u_eg_usat(\tau_u) + q_eg_qsat\left(\tau_q\right) + r_eg_rsat(\tau_r) + \sum\nolimits_{i=u,q,r}\left(\frac{\widetilde{g}_i\dot{\widehat{g}}_i}{\zeta_{gi}} + \frac{\widetilde{D}_{i+}\dot{\widehat{D}}_{i+}}{\zeta_{Di}} + \frac{\widetilde{\boldsymbol{\xi}}_i^T\dot{\widehat{\boldsymbol{\xi}}}_i}{\zeta_{\xi i}}\right) \\ &\le -k_1x_e^2 - k_2\left(\theta_e-\theta_{app}\right)^2 - k_3\left(\psi_e-\psi_{app}\right)^2 + y_ev_t\sin\psi_{app} - z_ev_t\sin\theta_{app} + \\ &\quad u_e\left(\widehat{\boldsymbol{\xi}}_{\boldsymbol{u}}^{\ T} - \widetilde{\boldsymbol{\xi}}_{\boldsymbol{u}}^{\ T}\right)\boldsymbol{S}_{\boldsymbol{u}}(x) + q_e\left(\widehat{\boldsymbol{\xi}}_{\boldsymbol{q}}^{\ T} - \widetilde{\boldsymbol{\xi}}_{\boldsymbol{q}}^{\ T}\right)\boldsymbol{S}_{\boldsymbol{q}}(x) + r_e\left(\widehat{\boldsymbol{\xi}}_{\boldsymbol{r}}^{\ T} - \widetilde{\boldsymbol{\xi}}_{\boldsymbol{r}}^{\ T}\right)\boldsymbol{S}_{\boldsymbol{r}}(x) + \\ &\quad u_eD_{u+} + q_eD_{q+} + r_eD_{r+} + u_eg_usat(\tau_u) + q_eg_qsat\left(\tau_q\right) + r_eg_rsat(\tau_r) + \\ &\quad \sum\nolimits_{i=u,q,r}\left(\frac{\widetilde{g}_i\dot{\widehat{g}}_i}{\zeta_{gi}} + \frac{\widetilde{D}_{i+}\dot{\widehat{D}}_{i+}}{\zeta_{Di}} + \frac{\widetilde{\boldsymbol{\xi}}_i^T\dot{\widehat{\boldsymbol{\xi}}}_i}{\zeta_{\xi i}}\right)\end{aligned} \tag{38}$$

Taking the pitch saturation term $q_eg_qsat(\tau_q)$ as an example, and assume a situation as $q_e<0$. According to the definition of control law in (30), the pitch control moment can be deducted as $\tau_q>0$. By recalling the control law in (30), the saturation term can be deduced as follows:

$$\begin{aligned}q_eg_qsat\left(\tau_q\right) &= -|q_e|g_q\frac{\tau_{q,max}}{\tau_q}\overline{\tau}_q\left(1+\widehat{g}_q\right) \\ &= -|q_e|g_q\widehat{g}_q\overline{\tau}_q\frac{\tau_{q,max}}{\tau_q} - |q_e|g_q\overline{\tau}_q\frac{\tau_{q,max}}{\tau_q} \\ &\le -|q_e|g_q\widehat{g}_q\overline{\tau}_q\end{aligned} \tag{39}$$

It is noted that properties $g_q>0$, $\overline{\tau}_q>0$ and $\frac{\tau_{q,max}}{\tau_q}\ge 1$ $(\forall\tau_q>0)$ have been used in the deduction of (39). The same deduction process can be followed for $q_e>0$, unsaturated and saturated situations respectively. Eventually, it can be concluded that $q_eg_qsat(\tau_q)\le -|q_e|g_q\widehat{g}_q\overline{\tau}_q\ \forall\ (r_e,\delta_r)\in\mathbb{R}^2$. Hence the saturation terms in surge and yaw directions can be concluded as follows: $u_eg_usat(\tau_u)\le -|u_e|g_u\widehat{g}_u\overline{\tau}_u$ and $r_eg_rsat(\tau_r)\le -|r_e|g_r\widehat{g}_r\overline{\tau}_r$.

According to the deduction in (39) and by recalling the control law in (30), (31) and (32), $\dot{V}_3$ can be further deduced as follows:

$$\begin{aligned}\dot{V}_3 &\le -k_1x_e^2 - k_2\left(\theta_e-\theta_{app}\right)^2 - k_3\left(\psi_e-\psi_{app}\right)^2 + \\ &\quad y_ev_t\sin\psi_{app} - z_ev_t\sin\theta_{app} + |u_e|\left\|\widehat{\boldsymbol{\xi}}_{\boldsymbol{u}}^{\ T}\boldsymbol{S}_{\boldsymbol{u}}\right| + |q_e|\left\|\widehat{\boldsymbol{\xi}}_{\boldsymbol{q}}^{\ T}\boldsymbol{S}_{\boldsymbol{q}}\right| + \\ &\quad \left|r_e\right\|\widehat{\boldsymbol{\xi}}_{\boldsymbol{r}}^{\ T}\boldsymbol{S}_{\boldsymbol{r}}\right| - u_e\widetilde{\boldsymbol{\xi}}_{\boldsymbol{u}}^{\ T}\boldsymbol{S}_{\boldsymbol{u}} - q_e\widetilde{\boldsymbol{\xi}}_{\boldsymbol{q}}^{\ T}\boldsymbol{S}_{\boldsymbol{q}} - r_e\widetilde{\boldsymbol{\xi}}_{\boldsymbol{r}}^{\ T}\boldsymbol{S}_{\boldsymbol{r}} + u_eD_{u+} + \\ &\quad q_eD_{q+} + r_eD_{r+} - |u_e|g_u\overline{\tau}_u\widehat{g}_u - |q_e|g_q\overline{\tau}_q\widehat{g}_q - |r_e|g_r\overline{\tau}_r\widehat{g}_r - \\ &\quad \frac{\widetilde{g}_u\widehat{g}_u^{-2}\dot{\widehat{g}}_u}{\zeta_{gu}} - \frac{\widetilde{g}_q\widehat{g}_q^{-2}\dot{\widehat{g}}_q}{\zeta_{gq}} - \frac{\widetilde{g}_r\widehat{g}_r^{-2}\dot{\widehat{g}}_r}{\zeta_{gr}} + \frac{\widetilde{D}_{u+}\dot{\widehat{D}}_{u+}}{\zeta_{Du}} + \\ &\quad \frac{\widetilde{D}_{q+}\dot{\widehat{D}}_{q+}}{\zeta_{Dq}} + \frac{\widetilde{D}_{r+}\dot{\widehat{D}}_{r+}}{\zeta_{Dr}} + \frac{\widetilde{\boldsymbol{\xi}}_{\boldsymbol{u}}^T\dot{\widehat{\boldsymbol{\xi}}}_{\boldsymbol{u}}}{\zeta_{\xi u}} + \frac{\widetilde{\boldsymbol{\xi}}_{\boldsymbol{q}}^T\dot{\widehat{\boldsymbol{\xi}}}_{\boldsymbol{q}}}{\zeta_{\xi q}} + \frac{\widetilde{\boldsymbol{\xi}}_{\boldsymbol{r}}^T\dot{\widehat{\boldsymbol{\xi}}}_{\boldsymbol{r}}}{\zeta_{\xi r}} \\ &\le -k_1x_e^2 - k_2\left(\theta_e-\theta_{app}\right)^2 - k_3\left(\psi_e-\psi_{app}\right)^2 + \\ &\quad y_ev_t\sin\psi_{app} - z_ev_t\sin\theta_{app} - k_4u_e^2 - k_5q_e^2 - k_6r_e^2 \\ &\le 0\end{aligned} \tag{40}$$

Since $\dot{V}_3\le 0$, and by recalling the definition on V_3 in (36), V_3 is a positive and monotonically decreasing function, $\lim_{t\to\infty}V_3$ exists. Then by recalling the Barbalat's lemma, it can be concluded that $\lim_{t\to\infty}\dot{V}_3=0$. Hence the kinematic and kinetic errors are asymptotically stable under actuator saturation, namely $\lim_{t\to\infty}\boldsymbol{d_e}=\boldsymbol{0}$, $\lim_{t\to\infty}(\psi_e,\theta_e)=(0,0)$ and $\lim_{t\to\infty}(u_e,q_e,r_e)=\boldsymbol{0}$. Hence, the control objectives in (12) can be realized based on kinematic controller (22) and kinetic controller in (30). □

3.4. Path-following algorithm

To provide better understanding and compact formulation of the proposed three-dimensional path-following control scheme, the pseudo code of the guidance law, kinematic and kinetic controllers are elaborated in Tab. 2. The numerical simulation studies in this paper are implemented aligning with Tab. 2. According to the complete control loop in control block diagram Fig. 2, the state vectors $\boldsymbol{\eta}$ and $\boldsymbol{\nu}$ can be obtained from on-board integrated navigation system. $x_p(\varpi)$, $y_p(\varpi)$ and $z_p(\varpi)$ are reference path functions that depend on the variable ϖ. Moreover, some constants have not been listed in Tab. 2, such as k_i and ζ_Δ. Furthermore, some iterative process such as integral calculations have not been listed in Tab. 2.

4. Numerical Examples

This section illustrates the effectiveness and robustness of the proposed path-following control scheme with two sets of numerical simulations. An 5.56-meters-long and 1089.8 kg AUV in Do and Pan (2009); McEwen and Streitlien (2001) is utilized. Model coefficients of the AUV are listed in Tab. 3. The under-actuated AUV has a minimum turning circle with a radius of 75m. Moreover, the saturated control forces and moments are given as follows:

$$\begin{cases}|\tau_u| \le \tau_{u-max} &= 2\times10^4\text{N} \\ |\tau_q| \le \tau_{q-max} &= 1.5\times10^4\text{Nm} \\ |\tau_r| \le \tau_{r-max} &= 1.5\times10^4\text{Nm}\end{cases} \tag{41}$$

The reference paths for two sets of numerical simulation are gives as straight path and three-dimensional helix respectively. For two cases, it can be assumed that the AUV is exposed to the unknown external disturbances with formulated equations as follows:

Table 2
Three-dimensional adaptive fuzzy path-following control algorithm of under-actuated AUVs.

Algorithm: 3-dimensional path following

Input : $x_p(\varpi), y_p(\varpi), z_p(\varpi), \eta, v, \psi_a, \theta_a, u_d$

$(\dot{x}_p, \dot{y}_p, \dot{z}_p) = (dx_p/d\varpi, dy_p/d\varpi, dz_p/d\varpi)\dot{\varpi}$

$\psi_p = atan2(\dot{y}_p, \dot{x}_p), \quad \theta_p = \arctan(-\dot{z}_p, \sqrt{\dot{x}_p^2 + \dot{y}_p^2})$

$\mathbf{d_e} = \mathbf{R_z}(\psi_\mathbf{p})\mathbf{R_y}(\theta_\mathbf{p})[\mathbf{x} - \mathbf{x_p}, \mathbf{y} - \mathbf{y_p}, \mathbf{z} - \mathbf{z_p}]^\mathbf{T}$

$\psi_{app} = -\psi_a(e^{k_\psi y_e} - 1)/(e^{k_\psi y_e} + 1), \quad \theta_{app} = \theta_a(e^{k_\theta z_e} - 1)/(e^{k_\theta z_e} + 1)$

Kinematic control law:

$q_d = -\dot{\alpha} + c_1\dot{s} + \dot{\theta}_{app} - k_2(\theta_e - \theta_{app}) - z_e v_t f(\theta_e, \theta_{app}) + z_e v_t f(\theta_e, \theta_{app})$

$r_d = \cos\theta(-\dot{\beta} + c_1\dot{s} + \dot{\psi}_{app} - k_3(\psi_e - \psi_{app})) - \cos\theta y_e v_t(\psi_e, \psi_{app})$

$\dot{\varpi} = (-v_t\cos(\theta_e)\cos(\theta_e) + k_1 x_e)/(\sqrt{\dot{x}_p^2 + \dot{y}_p^2 + \dot{z}_p^2})$

$\varpi = \varpi + \dot{\varpi}dt$

$u_e = u - u_d, \quad q_e = q - q_d, \quad r_e = r - r_e$

Kinetic control law:

$\dot{\widehat{D}}_{u+} = \zeta_{Du}|u_e|, \quad \dot{\widehat{\xi}}_u = \zeta_{\xi u}u_e S_u, \quad \dot{\widehat{D}}_{q+} = \zeta_{Dq}|q_e|, \quad \dot{\widehat{\xi}}_q = \zeta_{\xi q}q_e S_q$

$\dot{\widehat{D}}_{r+} = \zeta_{Dr}|r_e|, \quad \dot{\widehat{\xi}}_r = \zeta_{\xi r}r_e S_r$

$\bar{\tau}_u = \widehat{\xi}_u S_u + \widehat{D}_{u+} + k_4|u_e|, \quad \bar{\tau}_q = \widehat{\xi}_q S_q + \widehat{D}_{q+} + k_5|q_e|, \quad \bar{\tau}_r = \widehat{\xi}_r S_r + \widehat{D}_{r+} + k_6|r_e|$

$\dot{\widehat{g}}_u = \zeta_{gu}\widehat{g}_u^3|u_e|\bar{\tau}_u, \quad \dot{\widehat{g}}_q = \zeta_{gq}\widehat{g}_q^3|q_e|\bar{\tau}_q, \quad \dot{\widehat{g}}_r = \zeta_{gr}\widehat{g}_r^3|r_e|\bar{\tau}_r$

$\tau_u = -sign(u_e)\bar{\tau}_u(1 + \widehat{g}_u), \quad \tau_q = -sign(q_e)\bar{\tau}_q(1 + \widehat{g}_q), \quad \tau_r = -sign(r_e)\bar{\tau}_r(1 + \widehat{g}_r)$

Table 3
Parameters list of AUV nominal model.

$m = 1089.8$(kg)	$L = 5.56$m	$m_{11} = 1116$kg	$m_{22} = 2133$kg
$m_{33} = 2133$kg	$m_{44} = 36.7$kgm^2	$m_{55} = 4061$kgm^2	$m_{66} = 4061$kgm^2
$d_{11} = 25.5$kgs^{-1}	$d_{22} = 138$kgs^{-1}	$d_{33} = 138$kgs^{-1}	$d_{44} = 10$kgm^{2}s^{-1}
$d_{55} = 490$kgm^{2}s^{-1}	$d_{66} = 490$kgm^{2}s^{-1}	$d_{u2} = 0$	$d_{u3} = 0$
$d_{p2} = 0$	$d_{p3} = 0$	$d_{q2} = 0$	$d_{q3} = 0$
$d_{r2} = 0$	$d_{r3} = 0$	$d_{v2} = 920.1$kgm^{-2}s	$d_{v3} = 750$kgm^{-3}s^2
$d_{w2} = 920.1$kgm^{-2}s	$d_{w3} = 750$kgm^{-3}s^2		

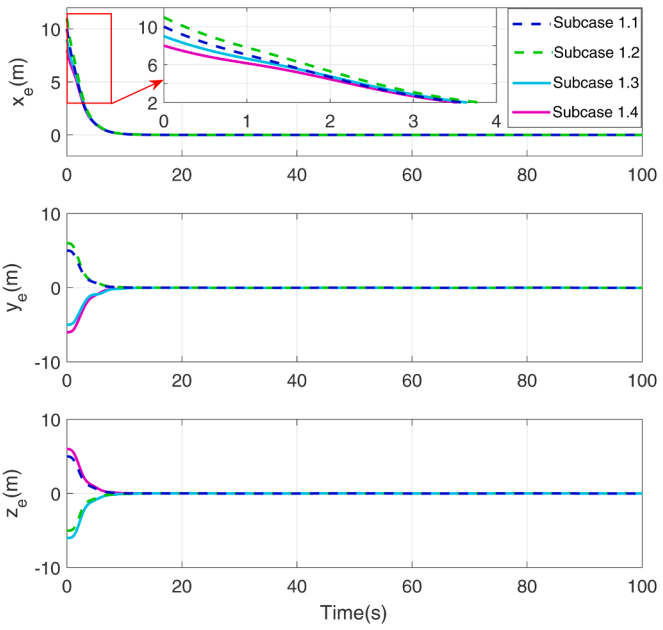

Fig. 4. Cross-tracking errors y_e, z_e and along-tracking errorx_e under 4 subcases.

$$\boldsymbol{\tau_d} = \begin{cases} \tau_{du} &= -0.2m_{11}d(t) \\ \tau_{dv} &= 0.1m_{22}d(t) \\ \tau_{dw} &= -0.1m_{33}d(t) \\ \tau_{dq} &= 0.1m_{55}d(t) \\ \tau_{dr} &= -0.2m_{66}d(t) \end{cases} \tag{42}$$

with $d(t) = 1 + 0.1\sin(0.2t)$ (Yu et al., 2017a). And the helix path is different from the straight path in that the path curvature and torsion are non-zero. Furthermore, some control parameters in Tab. 2 are given as follows: $\psi_a = \frac{\pi}{2}$, $\theta_a = \frac{\pi}{3}$, $k_\psi = 0.8$, $k_\theta = 0.5$, $k_1 = 0.5$, $k_2 = 1$, $k_3 = 1.5$, $\zeta_{Du} = 0.2$, $\zeta_{\xi u} = 0.2$, $\zeta_{gu} = 0.1$, $\zeta_{Dq} = 0.5$, $\zeta_{\xi q} = 0.1$, $\zeta_{gq} = 0.2$, $\zeta_{Dr} = 0.2$, $\zeta_{\xi r} = 0.1$, $\zeta_{gr} = 0.2$. For fuzzy logic approximation, seven nodes are used in both simulation cases.

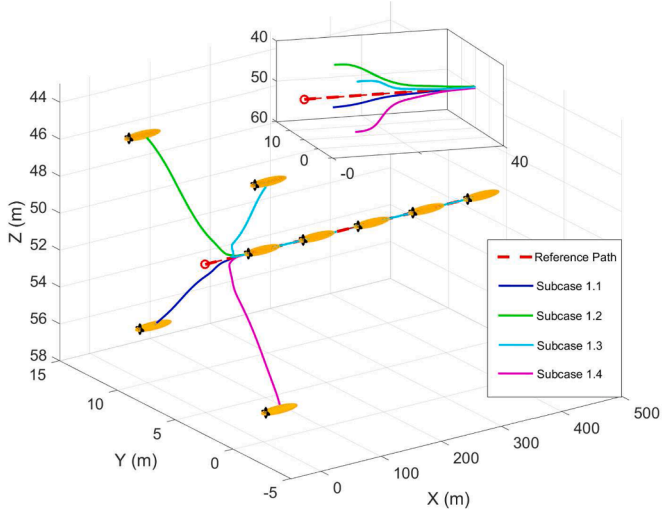

Fig. 3. 3-dimensional tracking results under Subcase 1.1, 1.2, 1.3 and 1.4.

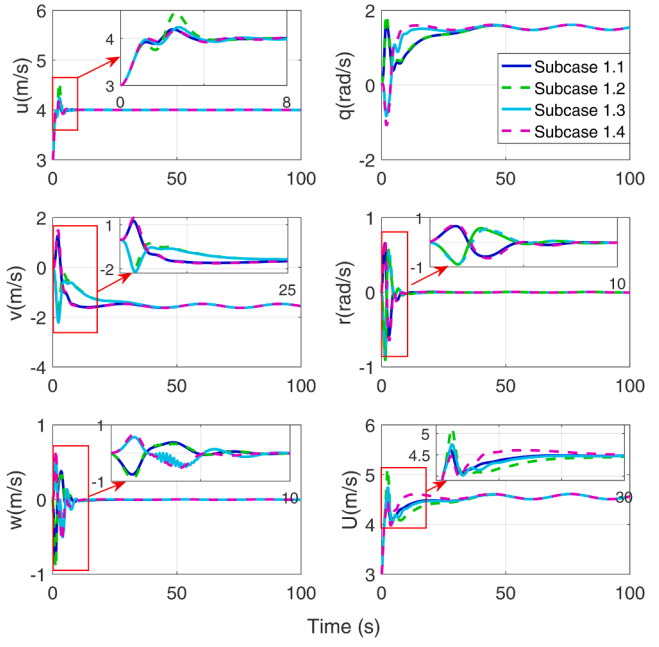

Fig. 5. AUV velocities under 4 subcases with desired surge velocity 4m/s.

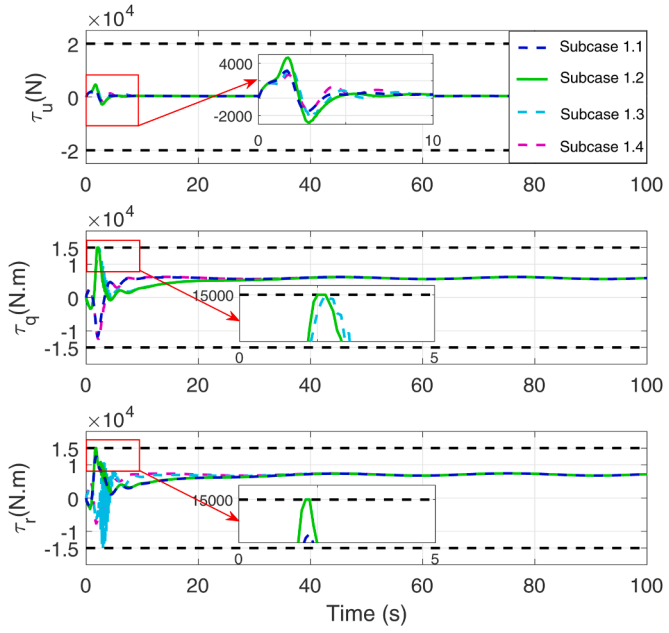

Fig. 6. Control force and moments of straight line tracking process under 4 subcases.

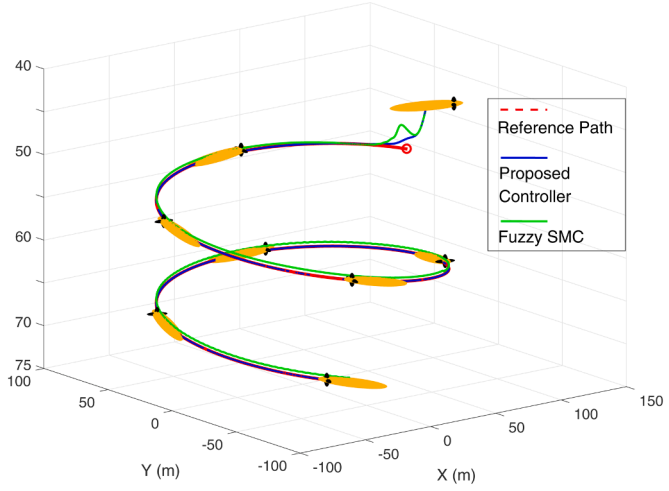

Fig. 7. 3-dimensional helix path-following result.

4.1. Case 1: Straight path following

The equation of the reference straight path is given as $y_p = 5\text{m}$, $z_p = 50\text{m}$. Let us set up 4 subcases under *Case* 1, where the vehicle is sailed from different inial position and posture. The initial position and posture vectors for four subcases are given as $\boldsymbol{\eta}_{1.1} = [10\text{m}, 10\text{m}, 55\text{m}, 0\text{rad}, 0\text{rad}]$, $\boldsymbol{\eta}_{1.2} = [11\text{m}, 11\text{m}, 45\text{m}, 0\text{rad}, 0\text{rad}]$, $\boldsymbol{\eta}_{1.3} = [9\text{m}, 0\text{m}, 44\text{m}, 0\text{rad}, 0\text{rad}]$ and $\boldsymbol{\eta}_{1.4} = [8\text{m}, -1\text{m}, 56\text{m}, 0\text{rad}, 0\text{rad}]$, respectively. The velocity vector is given as $\boldsymbol{v}_{1.1} = \boldsymbol{v}_{1.2} = \boldsymbol{v}_{1.3} = \boldsymbol{v}_{1.4} = [3\text{m/s}, 0\text{m/s}, 0\text{m/s}, 0\text{rad/s}, 0\text{rad/s}]$. The comparative three-dimensional path-following results are depicted in Fig. 3, where the red dashed line represents the reference path, and the blue, green, cyan, and black lines are the actual trajectory of AUV under subcase 1.1, 1.2, 1.3, and 1.4 respectively.

The path-following position errors, including the along-tracking error x_e, cross-tracking errors y_e and z_e, are shown in Fig. 4. It is proved that all of the path-following position errors are global asymptotical stable at origin.

The desired surge velocity under four subcases are given as $4m/s$. The velocities in the tracking process are depicted in Fig. 5. It is observed that the actual surge velocity converge to the desired velocity asymptotically. Due to the effect of time-varying ocean disturbance, the velocities on sway, heave, pitch and yaw directions are non-zero and time-varying. Moreover, the control force and moments are shown in Fig. 6. The control force τ_u and control moments τ_q and τ_r are strictly restricted between saturation intervals.

4.2. Case 2: 3-D Helix tracking

Helical diving process is simulated herein to test the performance and robustness of the proposed path-following control scheme. The equation of the reference helix path is given as $x_p = R\cos(c\varpi), y_p = R\sin(c\varpi), z_p = 50 + 0.5\varpi$ with $R = 80\text{m}$ and $c = 0.2618$. It is noted that the helix reference path is different from straight path in that the path curvature c_1 and torsion c_2 are non-zero constants. The initial AUV position and posture vector is given as $\boldsymbol{\eta} = [90\text{m}, -5\text{m}, 45\text{m}, -\pi/4\text{rad}, 3\pi/4\text{rad}]$. And the velocities vector is given as $\boldsymbol{v} = [3\text{m/s}, 0\text{m/s}, 0\text{m/s}, 0\text{rad/s}, 0\text{rad/s}]$. The numerical simulation duration is set as 200 seconds. And a sudden disturbance is imposed on the AUV at $100s - 105s$ with the term $d_{sudden} = 5 + 0.5\sin(0.2t)$, and the sudden disturbance force $\boldsymbol{\tau}_{\mathbf{d,sudden}}$ can be simulated with (42).

To verify the performance of the proposed control scheme, simulation case 2 compare the proposed control scheme with the model-based fuzzy sliding mode control (SMC). The fuzzy SMC considering the actuator saturation can be designed as follows Yu et al. (2018):

$$\begin{cases} \tau_{u,FSMC} &= \dfrac{1}{g_u}\left[\dot{u}_d - f_u - k_{1f}u_e - x_e\dfrac{\cos\theta_e\cos\psi_e}{\cos\alpha} - k_{2f}sgn(u_e)\right] - \widehat{\varrho}_u \\ \tau_{q,FSMC} &= \dfrac{1}{g_q}\left[\dot{q}_d - f_q - k_{3f}q_e - \theta_e + \theta_{app} - k_{4f}sgn(q_e)\right] - \widehat{\varrho}_q \\ \tau_{r,FSMC} &= \dfrac{1}{g_r}\left[\dot{r}_d - f_r - k_{5f}r_e - \psi_e + \psi_{app} - k_{6f}sgn(r_e)\right] - \widehat{\varrho}_r \end{cases} \tag{43}$$

where $k_{if}(i = 1\cdots6)$ are positive control parameters. $\widehat{\varrho}_u$, $\widehat{\varrho}_q$ and $\widehat{\varrho}_r$ are fuzzy approximation terms for saturated truncation in surge, pitch and yaw freedoms, which are given as $\widehat{\varrho}_j = \widehat{\boldsymbol{\xi}}_{jf}^T\boldsymbol{S}_{jf}$ with $(j = u, q, r)$. The control law for weight vectors are given as

$$\begin{cases} \dot{\widehat{\boldsymbol{\xi}}}_{uf}^T &= \dfrac{1}{\zeta_{uf}}g_u u_e \boldsymbol{S}_{uf} \\ \dot{\widehat{\boldsymbol{\xi}}}_{qf}^T &= \dfrac{1}{\zeta_{qf}}g_q q_e \boldsymbol{S}_{qf} \\ \dot{\widehat{\boldsymbol{\xi}}}_{rf}^T &= \dfrac{1}{\zeta_{rf}}g_r r_e \boldsymbol{S}_{rf} \end{cases} \tag{44}$$

where ζ_{uf}, ζ_{qf} and ζ_{rf} are positive control parameters. g_u, g_q, g_r, u_e, q_e and r_e are defined in the same way with that in subsection 3.2. The control

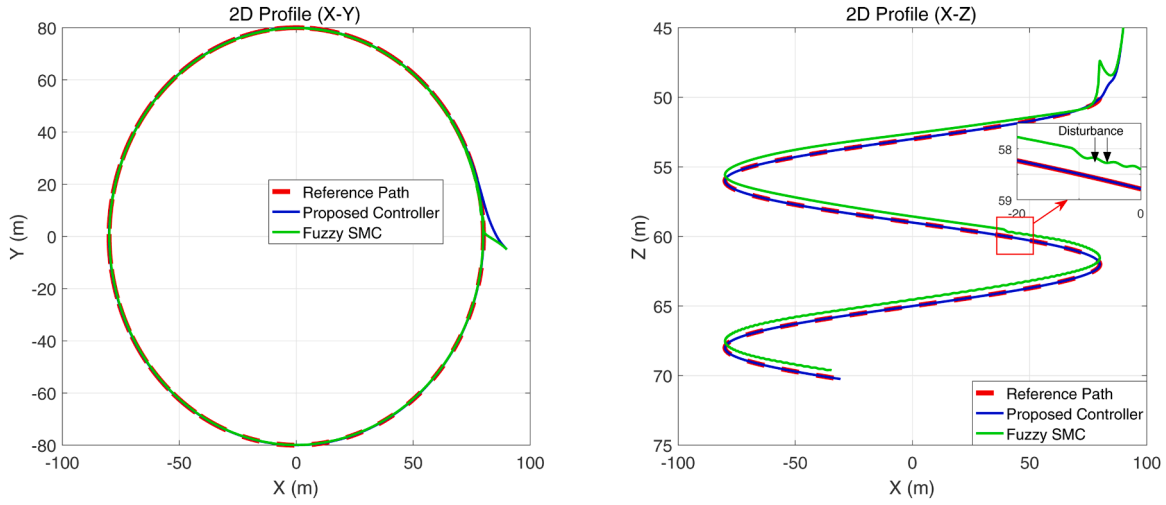

Fig. 8. 2-dimensional projection of reference path and AUV trajectory in X-Y and X-Z profiles.

parameters are given as: $k_{1f} = 0.5, k_{2f} = 0.1, k_{3f} = 0.5, k_{4f} = 0.1, k_{5f} = 0.8, k_{6f} = 0.5, \zeta_{uf} = 1.0, \zeta_{qf} = 0.5, \zeta_{rf} = 0.2$. The kinematic control law and corresponding control parameters of the control group are selected same with the proposed control scheme.

The comparative three-dimensional helix path following results are shown in Fig. 7. Further, the two-dimensional projection of the reference path and the AUV trajectories in X-Y and X-Z profiles are shown in Fig. 8. It is observed that the actual trajectory of the AUV with the proposed control scheme converges to the reference path asymptotically.

In addition, the along-tracking error x_e, cross-tracking errors y_e and z_e are depicted and compared in Fig. 9. The desired and actual pitch and yaw angles are presented in Fig. 10. It is noted that the desired pitch angle and yaw angle are given as $\theta_d = c_2\dot{s} - \alpha$ and $\psi_d = c_1\dot{s} - \beta$ respectively. Particularly, the enlarged views of path-following errors show details around the sudden disturbance. It can be observed that the path-following errors converge to 0 asymptotically. Comparatively, the proposed control scheme presents smaller steady-state errors and better dynamic performance. The desired travel speed is given as $4m/s$. The linear and angular velocities, sideslip angle β, and the angle of attack α in the tracking process are depicted and compared in Fig. 11. And the velocity errors are given in Fig. 12. It is noted that the desired pitch and yaw velocity are designed as shown in kinematic control law (22). The proposed control scheme presents better stability when the AUV was imposed sudden disturbance. In addition, the fuzzy logic system approximation targets and results are shown in Fig. 13. The approximation results are represented with $\boldsymbol{\xi_u S_u}$, $\boldsymbol{\xi_q S_q}$ and $\boldsymbol{\xi_r S_r}$ respectively. Furthermore, the comparative control force τ_u and control moments τ_q, τ_r are shown in Fig. 14, Particularly, the effect of the sudden disturbance on AUV have been depicted in Fig. 14. It can be observed that the control force and moments of proposed control scheme and fuzzy SMC are strictly constrained by the inherent actuator saturations. The proposed control scheme shows comparatively better actuator performance with the same simulation environment. The chattering effect of the actuators can be greatly avoided.

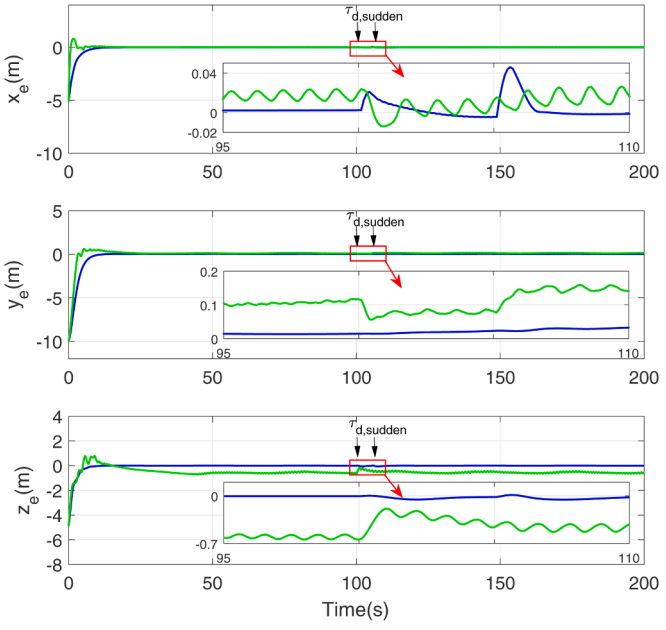

Fig. 9. Along-tracking error x_e, cross-tracking errors y_e and z_e under helix tracking case.

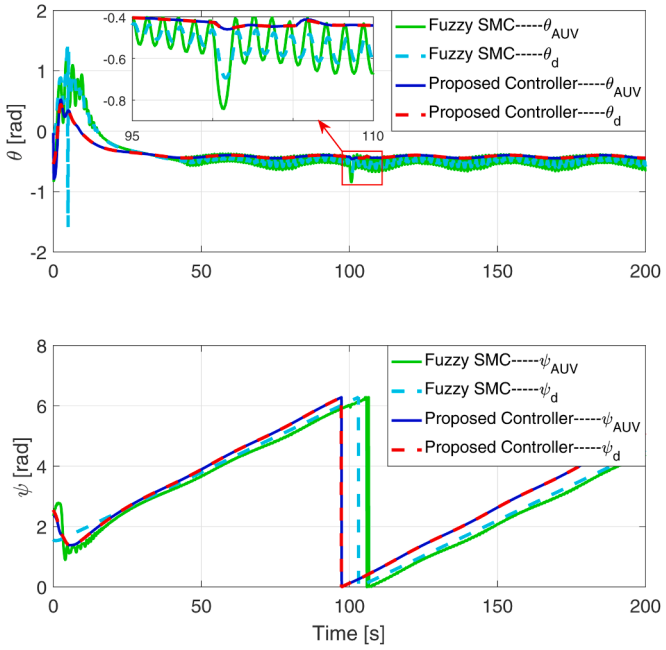

Fig. 10. Pitch and yaw angles for fuzzy SMC and proposed control scheme.

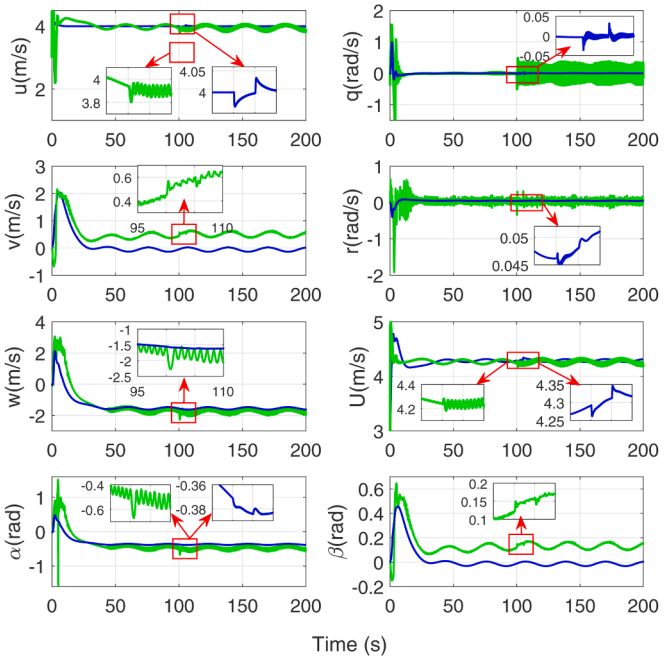

Fig. 11. AUV linear and angular velocities under helix tracking case with desired surge velocity 4m/s.

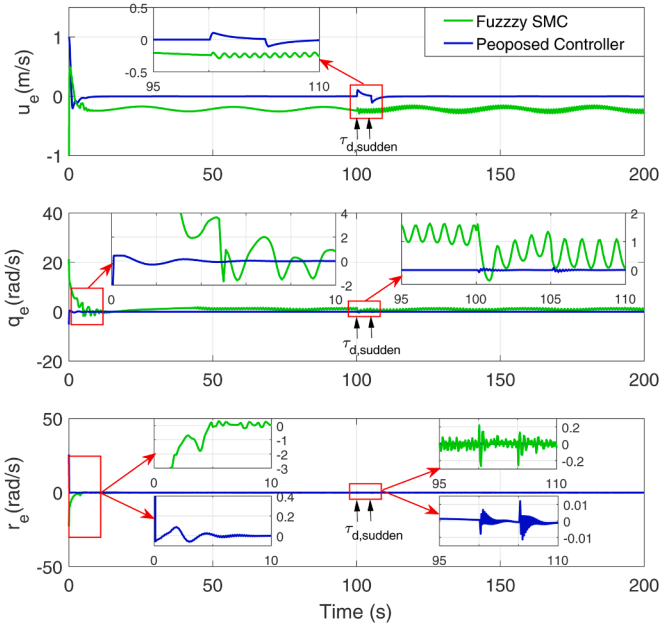

Fig. 12. Linear and angular velocity errors u_e, q_e and r_e.

5. Conclusion

In this paper, an adaptive approach-angle-based three-dimensional path-following control scheme is proposed for underactuated AUVs with unknown input saturations. The kinematic control law is designed based on the approach-angle-based guidance law, which synthesizes the cross-tracking errors into the tracking errors of heading and elevation angles. Further, the path-following error dynamic model is derived based on the theory of relative motion. The kinematic controller is designed by using the backstepping technique and Lyapunov theory to drive tracking errors asymptotically converge to 0. The kinetic control law is designed based on the indirect adaptive fuzzy logic control system, which is

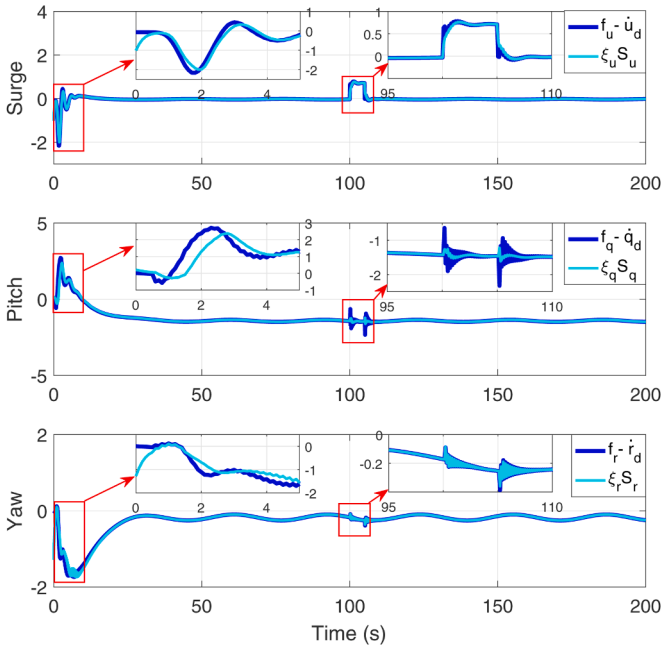

Fig. 13. Fuzzy logic system approximation results in surge, pitch and yaw freedoms.

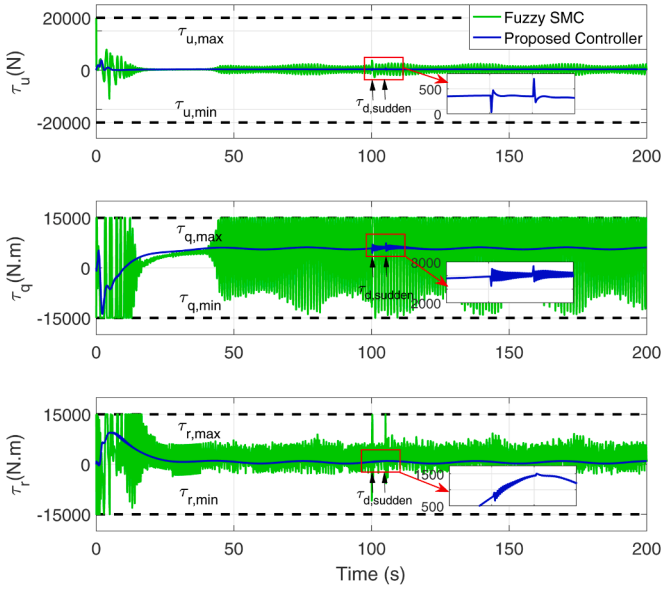

Fig. 14. Control force and moments for fuzzy SMC and proposed control scheme.

adopted to approximate the unknown functions including unknown coupled hydrodynamic parameters and complex differential of the desired pitch and yaw velocities. Furthermore, two adaptive laws are designed to estimate the constant AUV hydrodynamic parameters and unknown bounds of disturbance-like terms, which include the external disturbance and fuzzy approximation errors. Finally, two sets of numerical simulations for the straight path following with different initial position and spatial helix path following with sudden disturbance are implemented to demonstrate the effectiveness and robustness of the proposed control scheme. Control force and moments are strictly constrained in the pre-defined saturation zones. Moreover, simulation results on cross-tracking and along-tracking errors have correctly prove the tracking performance and asymptotic stability.

CRediT authorship contribution statement

Jialei Zhang: Conceptualization, Methodology, Visualization, Writing - original draft. **Xianbo Xiang:** Conceptualization, Writing - review & editing, Funding acquisition, Supervision, Resources. **Lionel Lapierre:** Validation, Writing - review & editing. **Qin Zhang:** Investigation, Visualization. **Weijia Li:** Formal analysis, Data curation.

Declaration of Competing Interest

The authors declare that they have no known competing financial interests or personal relationships that could have appeared to influence the work reported in this paper.

Acknowledgements

This work is supported by National Natural Science Foundation of China (under Grant 52071153), in part by the Shenzhen Science and Technology Plan Project (under Grant JCYJ20170413115305468), in part by the Fundamental Research Funds for the Central Universities (under Grant 2019JYCXJJ005).

Supplementary material

Supplementary material associated with this article can be found, in the online version, at 10.1016/j.apor.2020.102486

References

Alain, M., Claude, S., 1993. Trajectory tracking for unicycleltype and twolsteering wheels mobile robots. techreport. INIRA, Sophia-Antipolis, France.
Bingül, Z., Karahan, O., 2010. A fuzzy logic controller tuned with pso for 2 dof robot trajectory control. Expert Systems with Applications 38 (1), 1017–1031. https://doi.org/10.1016/j.eswa.2010.07.131.
Breivik, M., Fossen, T., 2005. Guidance-based path following for autonomous underwater vehicles. Proceedings of OCEANS 2005 MTS/IEEE. https://doi.org/10.1109/OCEANS.2005.1640200.
Chang, D., Edwards, C.R., Zhang, F., Sun, J., 2019. A data assimilation framework for data-driven flow models enabled by motion tomography. International Journal of Intelligent Robotics and Applications 3, 158–177. https://doi.org/10.1007/s41315-019-00092-5.
Chen, M., Zhu, D., 2019. Real-time path planning for a robot to track a fast moving target based on improved glasius bio-inspired neural networks. International Journal of Intelligent Robotics and Applications 3, 186–195. https://doi.org/10.1007/s41315-019-00082-7.
Chu, Z., Xiang, X., Zhu, D., Luo, C., Xie, D., 2019. Adaptive trajectory tracking control for remotely operated vehicles considering thruster dynamics and saturation constraints. ISA Transactions. https://doi.org/10.1016/j.isatra.2019.11.032.
Cui, R., Yang, C., Li, Y., Sharma, S., 2017. Adaptive neural network control of auvs with control input nonlinearities using reinforcement learning. IEEE Transactions on Systems, Man, and Cybernetics: Systems 47 (6), 1019–1029. https://doi.org/10.1109/TSMC.2016.2645699.
Cui, R., Zhang, X., Cui, D., 2016. Adaptive sliding-mode attitude control for autonomous underwater vehicles with input nonlinearities. Ocean Engineering 123, 45–54. https://doi.org/10.1016/j.oceaneng.2016.06.041.
Do, K.D., Pan, J., 2009. Control of ships and underwater vehicles: design for underactuated and nonlinear marine systems. Springer Science & Business Media.
Borhaug, K.Y.P.E., Pavlov, A., 2008. Integral los control for path following of underactuated marine surface vessels in the presence of constant ocean currents. 2008 47th IEEE Conference on Decision and Control, pp. 4984–4991. https://doi.org/10.1109/CDC.2008.4739352.
Sedrak, M.E.H.A, 1993. An experiment in linguistic synthesis with a fuzzy logic controller. Readings in Fuzzy Sets for Intelligent Systems 283–289. https://doi.org/10.1016/B978-1-4832-1450-4.50032-8.
Hussain, N.A.A., Arshad, M.R., Mohd-Mokhtar, R., 2011. Underwater glider modelling and analysis for net buoyancy, depth and pitch angle control. Ocean Engineering 38 (16), 1782–1791. https://doi.org/10.1016/j.oceaneng.2011.09.001.
Lapierre, L., Soetanto, D., 2007. Nonlinear path-following control of an auv. Ocean Engineering 34 (11-12), 1734–1744. https://doi.org/10.1016/j.oceaneng.2006.10.019.
Liu, L., Wang, D., Peng, Z., 2016. Path following of marine surface vehicles with dynamical uncertainty and time-varying ocean disturbances. Neurocomputing 173 (3), 799–808. https://doi.org/10.1016/j.neucom.2015.08.033.
Liu, Y., Liu, X., Jing, Y., 2019. Adaptive fuzzy finite-time stability of uncertain nonlinear systems based on prescribed performance. Fuzzy Sets and Systems 374, 23–39. https://doi.org/10.1016/j.fss.2018.12.015.
McEwen, R., Streitlien, K., 2001. Modeling and control of a variable-length auv. 12th International Symposium on Unmanned Untethered Submersible Technology.
Mišković, N., Bibuli, M., Birk, A., Caccia, M., Egi, M., Grammer, K., Marroni, A., Neasham, J., Pascoal, A., Vasilijević, A., et al., 2016. Caddy–cognitive autonomous diving buddy: Two years of underwater human-robot interaction. Marine Technology Society Journal 50 (4), 54–66. https://doi.org/10.4031/MTSJ.50.4.11.
Naik, M.S., Singh, S.N., 2007. State-dependent riccati equation-based robust dive plane control of auv with control constraints. Ocean Engineering 34 (11), 1711–1723. https://doi.org/10.1016/j.oceaneng.2006.10.014.
Nobile, M.S., Cazzaniga, P., Besozzi, D., Colombo, R., Mauri, G., Pasi, G., 2018. Fuzzy self-tuning pso: A settings-free algorithm for global optimization. Swarm and Evolutionary Computation 39, 70–85. https://doi.org/10.1016/j.swevo.2017.09.001.
Peng, Z., Wang, J., Wang, D., 2017. Distributed maneuvering of autonomous surface vehicles based on neurodynamic optimization and fuzzy approximation. IEEE Transactions on Control Systems Technology 26 (3), 1083–1090. https://doi.org/10.1109/TCST.2017.2699167.
Peng, Z., Wang, J., Wang, J., 2018. Constrained control of autonomous underwater vehicles based on command optimization and disturbance estimation. IEEE Transactions on Industrial Electronics 66 (5), 3627–3635. https://doi.org/10.1109/TIE.2018.2856180.
Popov, V.M., Georgescu, R., 1973. Hyperstability of Control Systems. Springer-Verlag Berlin Heidelberg, New York.
Precup, R.-E., David, R.-C., Petriu, E.M., 2016. Grey wolf optimizer algorithm-based tuning of fuzzy control systems with reduced parametric sensitivity. IEEE Transactions on Industrial Electronics 64 (1), 527–534. https://doi.org/10.1109/TIE.2016.2607698.
Qiao, L., Yi, B., Wu, D., Zhang, W., 2017. Design of three exponentially convergent robust controllers for the trajectory tracking of autonomous underwater vehicles. Ocean Engineering 134, 157–172. https://doi.org/10.1016/j.oceaneng.2017.02.006.
Sarda, E.I., Dhanak, M.R., 2019. Launch and recovery of an autonomous underwater vehicle from a station-keeping unmanned surface vehicle. IEEE Journal of Oceanic Engineering 44 (2), 290–299. https://doi.org/10.1109/JOE.2018.2867988.
Shojaei, K., 2016. Neural network formation control of underactuated autonomous underwater vehicles with saturating actuators. Neurocomputing 194, 372–384. https://doi.org/10.1016/j.neucom.2016.02.041.
Slotime, J.-J.E., Li, W., 1991. Applied nonlinear control. Prentice-Hall, Englewood Cliffs, NewJersey 07632.
Sun, B., Zhu, D., Yang, S.X., 2014. A bioinspired filtered backstepping tracking control of 7000-m manned submarine vehicle. IEEE Transactions on Industrial Electronics 61 (7), 3682–3693. https://doi.org/10.1109/TIE.2013.2267698.
Takagi, T., Sugeno, M., 1985. Fuzzy identification of systems and its applications to modeling and control. IEEE transactions on systems, man, and cybernetics SMC-15 (1), 116–132. https://doi.org/10.1109/TSMC.1985.6313399.
Tang, K., Man, K.F., Chen, G., Kwong, S., 2001. An optimal fuzzy pid controller. IEEE Transactions on Industrial Electronics 48 (1), 757–765. https://doi.org/10.1109/41.937407.
Vijay, M., Jena, D., 2017. Pso based neuro fuzzy sliding mode control for a robot manipulator. Journal of Electrical Systems and Information Technology 44 (1), 243–256. https://doi.org/10.1016/j.jesit.2016.08.006.
Wang, L.X., Mendel, J.M., 1992. Fuzzy basis functions, universal approximation, and orthogonal least-squares learning. IEEE Transactions on Neural Networks 3 (5), 807–814.
Wang, N., Ahn, C.K., 2019. Hyperbolic-tangent los guidance-based finite-time path following of underactuated marine vehicles. IEEE Transactions on Industrial Electronics. https://doi.org/10.1109/TIE.2019.2947845.
Wang, N., Su, S.F., Yin, J., Zheng, Z., Er, M.J., 2017. Global asymptotic model-free trajectory-independent tracking control of an uncertain marine vehicle: An adaptive universe-based fuzzy control approach. IEEE Transactions on Fuzzy Systems 26 (3), 1613–1625. https://doi.org/10.1109/TFUZZ.2017.2737405.
Wang, X., Su, H., Wang, X., Chen, G., 2017. Fully distributed event-triggered semiglobal consensus of multi-agent systems with input saturation. IEEE Transactions on Industrial Electronics 64 (6), 5055–5064. https://doi.org/10.1109/TIE.2016.2642879.
Wang, Z., Yang, S., Xiang, X., Vasilijević, A., Mišković, N., Nad¯, D., 2021. Cloud-based mission control of usv fleet: Architecture, implementation and experiments. Control Engineering Practice 106, 104657. https://doi.org/10.1016/j.conengprac.2020.104657.
Xiang, X., Yu, C., Zhang, Q., Wilson, P.A., Xu, G., 2020. Manoeuvring-based actuation evaluation of an auv with control surfaces and through-body thrusters. Applied Ocean Research 96, 102046. https://doi.org/10.1016/j.apor.2019.102046.
Xu, B., Huang, R., Li, M., 2016. Revise saturated activation functions. arXiv preprint arXiv:1602.05980.
Yu, C., Xiang, X., Lapierre, L., Zhang, Q., 2017. Nonlinear guidance and fuzzy control for three-dimensional path following of an underactuated autonomous underwater vehicle. Ocean Engineering. https://doi.org/10.1016/j.oceaneng.2017.10.001.
Yu, C., Xiang, X., Lapierre, L., Zhang, Q., 2017. Robust magnetic tracking of subsea cable by auv in the presence of sensor noise and ocean currents. IEEE Journal of Oceanic Engineering 43 (2), 311–322. https://doi.org/10.1109/JOE.2017.2768105.
Yu, C., Xiang, X., Wilson, P.A., Zhang, Q., 2020. Guidance-error-based robust fuzzy adaptive control for bottom following of a flight-style auv with saturated actuator dynamics. IEEE transactions on cybernetics 50 (5), 1887–1899. https://doi.org/10.1109/TCYB.2018.2890582.
Yu, C., Xiang, X., Zhang, Q., Xu, G., 2018. Adaptive fuzzy trajectory tracking control of an under-actuated autonomous underwater vehicle subject to actuator saturation.

International Journal of Fuzzy Systems 20 (1), 269–279. https://doi.org/10.1007/s40815-017-0396-9.

Zhang, Q., Zhang, J., Chemori, A., Xiang, X., 2018. Virtual submerged floating operational system for robotic manipulation. Complexity 1–18. https://doi.org/10.1155/2018/9528313.

Zheng, Z., Huang, Y., Xie, L., Zhu, B., 2018. Adaptive trajectory tracking control of a fully actuated surface vessel with asymmetrically constrained input and output. IEEE Transactions on Control Systems Technology 26 (5), 1851–1859. https://doi.org/10.1109/TCST.2017.2728518.

Zheng, Z., Sun, L., 2015. Path following control for marine surface vessel with uncertainties and input saturation. Neurocomputing 177, 158–167. https://doi.org/10.1016/j.neucom.2015.11.017.

Zuo, Z., Cheng, L., Wang, X., Sun, K., 2019. Three-dimensional path-following backstepping control for an underactuated stratospheric airship. IEEE Transactions on Aerospace and Electronic Systems 55 (3), 1483–1497. https://doi.org/10.1109/TAES.2018.2873054.